From Eqs. (9) and (10), we have

$$\eta=\frac{2}{\sqrt{\pi}}\frac{\psi}{(1-\psi)^m}\left[1+\sum_{j=1}^{\infty}a_j(1-\psi)^j\right] \tag{16}$$

Substituting Eq. (16) into Eq. (14) and integrating its result, then we finally get

$$\begin{aligned}\tau=\int_0^{\psi}\Bigg\{&\left(M+\sum_{j=1}^{\infty}b_jN_j\right)2\psi\left[1+\sum_{j=1}^{\infty}a_j(1-\psi)^j\right]\\&\times\Bigg(\left[(1-\psi)^m-u_e^m\right]\left\{1+\sum_{j=1}^{\infty}a_j\left[(1-\psi)^j-j\psi(1-\psi)^{j-1}\right]\right\}\\&+m\psi\left[1+\sum_{j=1}^{\infty}a_j(1-\psi)^j\right](1-\psi)^{m-1}\Bigg)+\sqrt{\pi}\psi\left(P+\sum_{j=1}^{\infty}b_jQ_j\right)\\&\times\left[1+\sum_{j=1}^{\infty}a_j(1-\psi)^j\right]^2\left[(1-\psi)^m-u_e^m\right]\Bigg\}\\&\div\pi\left[(1-\psi)^m-u_e^m\right]^3\left(M+\sum_{j=1}^{\infty}a_jN_j+\frac{1}{\sqrt{\pi}}\sum_{j=1}^{\infty}ja_jL_j\psi\right)\mathrm{d}\psi\end{aligned} \tag{17}$$

For the case of constant thermal properties, the solution of Eq. (17) becomes

$$m=4\quad \tau=0.31831(1-\psi)^{-8}-0.57203(1-\psi)^{-7}+0.24294(1-\psi)^{-6}+0.01528 \tag{18}$$

$$m=1\quad \tau=0.31831(1-\psi)^{-2}-0.18445(1-\psi)^{-1}+0.45217\ln(1-\psi)-0.13386 \tag{19}$$

The surface temperature histories and internal temperature distribution which are expressed in closed analytical form are shown in Figs. 1 and 2, and compared with other available solutions.[1,2,8] The agreement is good in both cases and all of the curve no distinction between the results is evident.

In another special case, the thermal conductivity and heat capacity are assumed to be a linear function of the temperature

$$k(\theta)=1+a(1-\theta) \tag{20}$$

$$u(\theta)=1+b(1-\theta) \tag{21}$$

The solution of Eq. (17) becomes

$$\begin{aligned}\tau=\int_0^{\psi}\Bigg\{&\psi[0.22030(1+b\psi)-0.06758b\psi]\\&\times[1+a(1-\psi)]\{[(1-\psi)^m-u_e^m][1+a(1-2\psi)]\\&+m\psi[1+a(1-\psi)](1-\psi)^{m-1}\}+\psi[0.15647(1+b\psi)\\&-0.06000b\psi][1+a(1-\psi)]^2[(1-\psi)^m-u_e^m]\Bigg\}\\&\div[0.34605(1+a\psi)+0.07251a\psi][(1-\psi)^m-u_e^m]^3\mathrm{d}\psi\end{aligned} \tag{22}$$

The surface temperature histories for $m=4$; $a=+0.5$, 0, -0.5; and $b=+0.5$, 0, -0.5 are shown in Fig. 3 and compared with numerical solutions and integral solutions.[3] The agreement was found to be good. It is interesting to note that the cooling of the semi-infinite body proceeds more slowly in the case $a>0$ and $b>0$.

Remarks

For the case of material property variations, both the thermal conductivity and heat capacity can be expressed in terms of power series of variable temperature. The surface temperature history obtained by the variational embedding technique is in integral form. However, the solution becomes closed form for the constant thermal property case. The results of all considered cases have been presented in graphical form and comparisons have been made with other solutions. Agreement was found to be good. From the results of the analysis, it appears that the present technique is a simple, fast and straightforward method. In addition to the accuracy, the variational embedding technique has been shown to provide a systematic means of deducing the surface temperature history for one-dimensional nonlinear heat transfer problems.

References

[1] Abarbanel, S. S., "Time Dependent Temperature Distribution in Radiating Solids," *Journal of Mathematical Physics,* Vol. 39, 1960, pp. 246-257.

[2] Lardner, T. L., "Biot's Variational Principle in Heat Conduction," *AIAA Journal,* Vol. 1, Jan. 1961, pp. 196-206.

[3] Chung, B. T. F. and Yeh, L. T., "Analysis of Heat Transfer in Slabs with Variable Properties Subjected to Radiation and Convection," ASME Paper 75-WA/HT-67, 1975.

[4] Chambre, P. L., "Nonlinear Heat Transfer Problem," *Journal of Applied Physics,* Vol. 30, Nov. 1959, pp. 1683-1688.

[5] Crosbie, A. L. and Viskanta, R., "Transient Heating or Cooling of One-Dimensional Solids by Thermal Radiation," *Proceedings of the Third International Heat Transfer Conference*, Vol. 5, Aug. 1966, pp. 146-153.

[6] Edelem, D. G. B., *Nonlocal Variations and Local Invariance of Fields,* Elsevier, New York, 1969.

[7] Bhatkar, V. P. and Rao, B., "Variational Embedding Method and Application to Distributed Systems Control," *International Journal of Control,* Vol. 23, 1976, pp. 805-820.

[8] Carslaw, H. S. and Jaeger, J. C., *Conduction of Heat in Solids,* 2nd ed., Oxford University Press, 1959.

Evaluation of Total Body Heat Transfer in Hypersonic Flow

Richard L. Baker* and Raymond F. Kramer†
The Aerospace Corporation, El Segundo, California

Introduction

THE purpose of this Note is to provide analytic equations and calculated numerical results to enable quick and accurate evaluation of the total heat transfer to a conical body in a hypersonic flow environment. From such information, thermal protection system requirements for conical bodies in hypersonic flowfields can be determined.

Local Heat-Transfer Rates

An expression is needed for the total integrated heat transfer in hypersonic flow environments as a function of appropriate flowfield, body scale, and body geometry parameters. First, an expression is required for the local heat-transfer coefficient. In Refs. 1 and 2, the boundary-layer integral momentum equation is solved, and Reynolds analogy and a compressibility transformation are applied to obtain the

Received Dec. 21, 1981.

*Engineering Specialist, Vehicle Engineering Division.

†Manager, Reentry Applications Section, Information Processing Division.

following expressions for the local heat-transfer coefficient:

Laminar

$$C_H = \dot{q}^L / \rho_e u_e H_0 = 0.470 r \mu_e \Big/ \left(2\int_0^s \rho_e u_e \mu_e r^2 \mathrm{d}s\right)^{1/2} \tag{1a}$$

Turbulent

$$C_H = \dot{q}^T / \rho_e u_e H_0 = 0.0288 r^{1/4} \mu_e \Big/ \mu_0^{3/5} \left(\int_0^s \rho_e u_e \mu_e r^{5/4} \mathrm{d}s\right)^{1/5} \tag{1b}$$

These expressions have been found to agree very closely with experimental data at high supersonic Mach numbers[3] and at moderate hypersonic Mach numbers.[4]

If the following nondimensional quantities are defined

$$\bar{\rho}_e = \rho_e/\rho_0, \qquad \bar{r} = r/r_B$$

$$\bar{\mu}_e = \mu_e/\mu_0, \qquad \bar{s} = s/r_B$$

$$\bar{u}_e = u_e/\sqrt{2H_0}, \qquad \tau = 2r_B/L = d/L \tag{2}$$

then the local heat-transfer coefficient expressions become

$$C_H = C_1 \bar{r}^n \bar{\mu}_e \Big/ \left[\left(\int_0^{\bar{s}} \bar{\rho}_e \bar{u}_e \bar{\mu}_e \bar{r}^{n+1} \mathrm{d}\bar{s}\right)^{n/(n+1)}\right] \times \left(\frac{\mu_0}{\rho_0 (2H_0)^{1/2} r_B}\right)^{n/(n+1)} \tag{3}$$

where for laminar flow $C_1 = 0.332$, $n = 1$ and for turbulent flow $C_1 = 0.0288$, $n = 1/4$. In Eqs. (2), subscripts e and 0 refer to boundary-layer edge and stagnation conditions, respectively. Also, r_B and L are the base radius and length, respectively.

Integrated Heat-Transfer Expressions

An integration must now be performed over the surface area to obtain the total heat-transfer rate $\mathrm{d}Q/\mathrm{d}t$.

$$\mathrm{d}Q/\mathrm{d}t = \int\int_S \dot{q}\,\mathrm{d}S = 2\pi \int_0^s \dot{q} r \mathrm{d}s \tag{4}$$

This yields, upon substitution from Eqs. (1) and (2),

$$\frac{\mathrm{d}Q/\mathrm{d}t}{\rho_\infty V_\infty H_0 (\pi r_B^2)} = 2(\gamma+1)/(\gamma-1) \int_0^s \bar{\rho}_e \bar{u}_e C_H \bar{r} \mathrm{d}\bar{s} \tag{5}$$

The hypersonic approximations $\sqrt{2H_0} \approx V_\infty$ and $\rho_0/\rho_\infty = (\gamma+1)/(\gamma-1)$ have been made in obtaining Eq. (5). When Eq. (3) is substituted into Eq. (5), the resulting equation may be integrated[5] easily to obtain

$$\frac{\mathrm{d}Q/\mathrm{d}t}{\rho_\infty V_\infty H_0 (\pi r_B^2)} = \frac{2(n+1) C_1 (\gamma+1)/(\gamma-1)}{[Re_0]^{n/(n+1)}} I_Q^{1/(n+1)} \tag{6}$$

where a shock-layer Reynolds number and heat-transfer integral are given by

$$Re_0 = \rho_0 (2H_0)^{1/2} r_B/\mu_0 \tag{7}$$

$$I_Q = \int_0^{\bar{s}} \bar{\rho}_e \bar{u}_e \bar{\mu}_e \bar{r}^{n+1} \mathrm{d}\bar{s} \tag{8}$$

Substituting the appropriate values for C_1 and n, we obtain

Laminar:

$$\mathrm{d}Q^L/\mathrm{d}t \Big/ \rho_\infty V_\infty H_0 (\pi r_B^2) = 1.328(\gamma+1)/(\gamma-1)\,(I_Q^L)^{1/2} Re_0^{-1/2} \tag{9a}$$

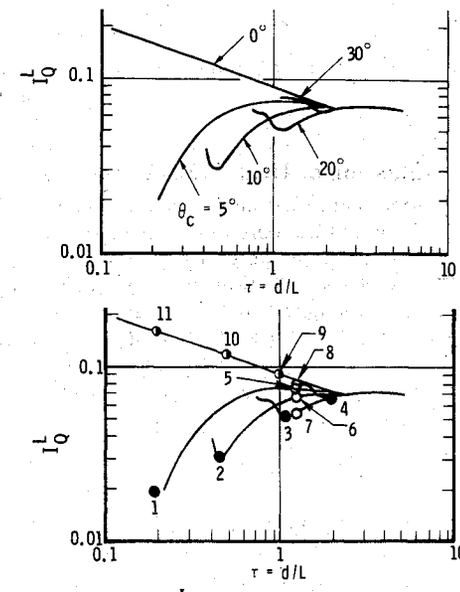

Fig. 1 I_Q^L vs τ for sphere cones.

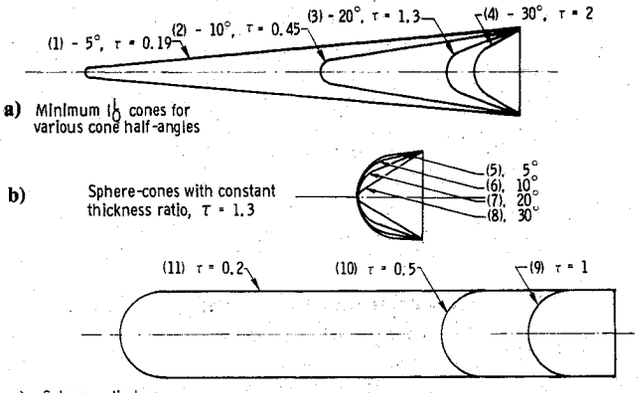

Fig. 2 Parametric shape variation.

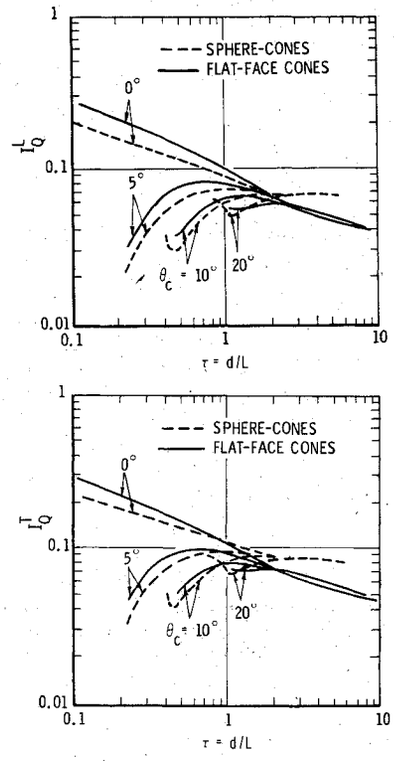

Fig. 3 I_Q vs τ for sphere cones and flat-face cones.

Turbulent:

$$dQ^T/dt\Big/\rho_\infty V_\infty H_0(\pi r_B^2)=0.0720(\gamma+1)/(\gamma-1)\,(I_Q^T)^{4/5}Re_0^{-1/5} \tag{9b}$$

Evaluation of Heat-Transfer Integrals

The total nondimensional heat-transfer rates given by Eqs. (9) can be interpreted as representing the fraction of the intercepted freestream total energy flux which is transferred as heat to the body. These equations are applicable for all body shapes. However, the heat-transfer integral I_Q depends upon the shape contour of the body. The evaluation of I_Q involves computation of the local pressure p_e at each position on the body since, in terms of the normalized pressure $\bar{p}_e=p_e/p_0$, $\bar{\rho}_e\bar{\mu}_e$ is given by

$$\bar{\rho}_e\bar{\mu}_e=\rho_e\mu_e/\rho_0\mu_0=\bar{p}_e^{\,[(\gamma-1)\omega+1]/\gamma} \tag{10}$$

Also, when an isentropic expansion is assumed, the local velocity $\bar{u}_e$ can be written in terms of $\bar{p}_e$ as

$$\bar{u}_e=u_e/\sqrt{2H_0}=\sqrt{1-\bar{p}_e^{(\gamma-1)/\gamma}} \tag{11}$$

Thus, I_Q is a function of the specific heat ratio γ, the temperature exponent in the viscosity law ω, and the body geometry ($\gamma=1.2$, $\omega=1.0$ in this work).

The pressure distributions were obtained from numerical inviscid flowfield calculation procedures.[6-8] Calculations were carried out for cone half-angles θ_c of 30, 20, 10, 5 and 0 deg. Results of the computations for these geometries were then used to evaluate the integrand of Eq. (8) along the body. The I_Q^L and I_Q^T for each cone half-angle and a range of thickness ratio, $\tau=d/L$, were evaluated.

Parametric Variation of I_Q^L for Sphere Cones

Calculated values of I_Q^L as a function of τ for laminar flow over sphere cones are shown for various cone half-angles in Fig. 1a. For each cone half-angle greater than zero, the curves of I_Q^L vs τ pass through a minimum. The minimum I_Q^L decreases as θ_c decreases. To illustrate the effects of cone half-angle and thickness ratio on the total heat-transfer rate, consider the cones represented by the circles in Fig. 1b, i.e., selected points on Fig. 1a.

Each of the ● symbols represents the minimum in the curve of I_Q^L vs τ for a particular cone half-angle. Shown in Fig. 2a are four cones, having a constant base radius and with cone half-angles, thickness ratios, and bluntness ratios corresponding to points 1-4. Since the base radius r_B is constant, the intercepted freestream total energy flux is constant. However, the fraction of this flux transferred as heat to the body decreases monotonically as the cone half-angle and thickness ratio decrease: thus, $dQ_4/dt>dQ_3/dt>dQ_2/dt>dQ_1/dt$.

The ○ symbols in Fig. 1b represent cones having a constant thickness ratio of 1.3. These cones are illustrated in Fig. 2b. The 20 deg cone, represented by point 7, has the lowest heat-transfer rate. The 5 and 10 deg cones (points 5 and 6) have higher heat-transfer rates because of larger areas associated with the high heat-transfer nose cap. However, the 30 deg cone (point 8) has the highest heat-transfer rate because of the high conical pressure on the cone surface. Thus, for these cones, $dQ_8/dt>dQ_5/dt>dQ_6/dt>dQ_7/dt$.

The behavior of I_Q vs τ for a sphere cylinder can now be understood by considering Fig. 2c and the ◑ symbols in Fig. 1b. In Fig. 2c, bodies 9 and 10 may be considered parts of body 11. Therefore, going from body 9 to 10 and then to 11, the total heat-transfer must increase or $dQ_{11}/dt>dQ_{10}/dt>dQ_9/dt$.

Calculated I_Q for Sphere Cones and Flat-Face Cones

Numerical values of I_Q for sphere cones and flat-face cones are shown for laminar and turbulent flow in Figs. 3a and 3b, respectively. In general, for $\tau>2$, $(I_Q)_{\text{flat-face cone}}<(I_Q)_{\text{sphere cone}}$ and for $\tau<2$, $(I_Q)_{\text{flat-face cone}}>(I_Q)_{\text{sphere cone}}$. For $\tau>2$, the maximum increase in I_Q for a sphere cone compared to a flat-face cone having the same τ is about 50%. For $\tau<2$, the flat-face cone I_Q values are 5-30% greater than the sphere cone values. The reasons for this comparative behavior are directly related to the surface pressure distributions. The relatively low heat-transfer rates on a flat face and very low local pressures on the forward frustum part of a flat-face cone account for an I_Q less than that for a sphere cone with the same thickness ratio. However, as τ decreases, higher flat-face cone local pressure values on the mid and rearward frustum eventually result in $(I_Q)_{\text{flat-face cone}}$ becoming greater than $(I_Q)_{\text{sphere cone}}$.

Summary

Beginning with the hypersonic convective heat-transfer expressions for laminar and turbulent flow given by Vaglio-Laurin,[1,2] equations for the total heat transfer to a body in a hypersonic flow environment have been derived.[9] When these equations are used together with the graphical results presented, total heat transfer to selected conical body geometries can be calculated directly. The total heat transfer is given as a function of freestream parameters, body scale, and heat-transfer integrals which are functions of the body geometry. Inviscid numerical calculation methods for surface pressure distributions were used to evaluate the laminar and turbulent heat-transfer integrals I_Q^L and I_Q^T for 0, 5, 10, 20, and 30 deg sphere cones and flat-face cones.

Acknowledgments

This study was supported by the Space Division, U. S. Air Force Systems Command under Contract F04701-76-C-0077.

References

[1] Vaglio-Laurin, R., "Laminar Heat Transfer on Three-Dimensional Blunt Nosed Bodies in Hypersonic Flow," *ARS Journal,* Vol. 29, Feb. 1959, pp. 123-129.

[2] Vaglio-Laurin, R., "Turbulent Heat Transfer on Blunt Nosed Bodies in Two-Dimensional and General Three-Dimensional Hypersonic Flow," *Journal of the Aero/Space Sciences,* Vol. 27, Jan. 1960, pp. 27-36.

[3] Widhopf, G. F. and Hall, R., "Transitional and Turbulent Heat Transfer Measurements on a Yawed Blunt Conical Nose Tip," *AIAA Journal,* Vol. 10, Oct. 1972, pp. 1318-1325.

[4] Crowell, P. G., personal communication, The Aerospace Corp., El Segundo, Calif., 1977.

[5] Aihara, Y., "Optimum Body Geometries of Minimum Heat Transfer at Hypersonic Speeds," *AIAA Journal,* Vol. 6, Nov. 1968, pp. 2187-2188.

[6] Masson, B. S., Taylor, T. D., and Foster, R. M., "Application of Godunov's Method to Blunt Body Calculations," *AIAA Journal,* Vol. 7, April 1969, p. 694.

[7] Baker, R. L., "Method of Characteristics Computer Program Including Embedded Shocks and Total Enthalpy Gradients Normal to Streamlines," The Aerospace Corp., El Segundo, Calif., Rept. TOR-0080(5550-01)-1, Jan. 31, 1980.

[8] Inouye, M., Rakich, J. V., and Lomax, H., "A Description of Numerical Methods and Computer Programs for Two-Dimensional and Axisymmetric Supersonic Flow over Blunt-Nosed and Flared Bodies," NASA TN-D-2970, Aug. 1965.

[9] Baker, R. L. and Kramer, R. F., "Evaluation of Total Heat Transfer in Hypersonic Flow Environments," The Aerospace Corp., El Segundo, Calif., Rept. SAMSO-TR-78-20, Oct. 1978.